



# Investigating the role of faults in fluid migration and gas hydrate formation along the southern Hikurangi Margin, New Zealand

Jess I. T. Hillman<sup>1</sup> · Gareth J. Crutchley<sup>2</sup> · Karsten F. Kroeger<sup>1</sup>

Received: 21 July 2019 / Accepted: 26 January 2020 / Published online: 7 March 2020  
© Springer Nature B.V. 2020

## Abstract

The Hikurangi Margin off the east coast of the North Island (Te Ika-a-Māui) is a tectonically active subduction zone and the location of New Zealand's largest gas hydrate province. Faults are internally complex volumetric zones that may play a significant role in the migration of fluids beneath the seafloor. The combined processes of deformation and fluid migration result in the formation of concentrated hydrate accumulations along accretionary ridges. It is not fully understood to what extent faults control fluid migration along the Hikurangi Margin, and whether deep-seated thrust faults provide a pathway for thermogenic gas to migrate up from sources at depth. Using 2D models based on seismic data from the region we investigated the role of thrust faults in facilitating fluid migration and contributing to the formation of concentrated gas hydrates. By altering permeability properties of the fault zones in these transient state models we can determine whether faults are required to act as fluid flow pathways. In this study we focus on two study sites offshore southern Wairarapa, using realistic yet simplified fault geometries derived from 2D seismic lines. The results of these models allow us to start to disentangle the complex relationship between fault zone structure, permeability, geometry, fluid migration and gas hydrate formation. Based on the model outputs we propose that faults act as primary pathways facilitating fluid migration and are critical in the formation of concentrated gas hydrate deposits.

**Keywords** Gas hydrate · Faults · Fluid migration · Modelling · Seismic data

## Introduction

Fluid migration through sediments is a key factor in the formation of gas hydrates. Hydrate formation in the gas hydrate stability zone (GHSZ) is facilitated by gas and/or fluid migration via either short or long range mechanisms (Malinverno and Goldberg 2015; Nole et al. 2016; Taladay et al. 2017). Gas migration can occur as a result of steady flow along permeable pathways in dipping strata or as episodically focused fluid flow along highly permeable pathways such as faults. Deep penetrating faults in subduction margins may act as conduits for fluid flow from depth, and are frequently associated with the formation of folded anticlinal ridges due to shortening of the accretionary wedge

(Pecher et al. 2010; Johnson et al. 2015). Fluid flow alternates between diffuse and focused flow over time, depending on the stress field (Taladay et al. 2017). In a subduction margin setting fluid flow will be variable over geological timescales, and will also be impacted by the dewatering of the accretionary wedge during sediment compression (Johnson et al. 2015). Expulsion of fluids from the overpressured accretionary prism and/or from seismic and slow slip events could both potentially supply gas generated at depth to the GHSZ (Johnson et al. 2015; Taladay et al. 2017). As a result, deep seated faults along seismically active subduction margins are a key factor in fluid migration and the formation of gas hydrates.

The Hikurangi Margin is an active subduction zone off the east coast of New Zealand's North Island (Te Ika-a-Māui), where the Pacific plate subducts beneath the Australian plate. It is also New Zealand's largest gas hydrate province, with bottom simulating reflections (BSRs) abundant in water depths > 600 m (Pecher et al. 2005; Navalpakam et al. 2012). Previous studies have found that faults appear to play a role in fluid and/or gas migration towards

✉ Jess I. T. Hillman  
j.hillman@gns.cri.nz

<sup>1</sup> GNS Science, 1 Fairway Drive, Avalon 5040, New Zealand

<sup>2</sup> GEOMAR Helmholtz Centre for Ocean Research,  
Wischofstrasse 1-3, 24148 Kiel, Germany

the GHSZ along the Hikurangi Margin (e.g., Crutchley et al. 2015; Wang et al. 2017). Deep-seated thrust faults and shallower normal and backthrust faults are ubiquitous across the region due to deformation at the plate boundary. It is not yet clear; however, whether the faults themselves act as the main conduits for fluid migration, or whether other factors such as primary porosity of the sedimentary strata, and secondary porosity due to fracturing are more important. Such details are important when considering the distribution of concentrated hydrate deposits and modelling gas production from hydrates, due to the potential for faults to compartmentalise flow and restrict flow pathways.

Seismic observations by Wang et al. (2017) suggest that faults imaged inboard of Pōrangahau Ridge on the Hikurangi Margin (Fig. 2) may be impermeable, with high concentrations of gas hydrates restricted to one side, thereby indicating that fluid and/or gas flow across the fault zone is limited. Resolving the internal structure of fault zones in seismic data is problematic due to the limited resolution. As is expected on all deforming accretionary wedges (e.g., Morley et al. 2011), thrust faults along the Hikurangi Margin are associated with hanging wall anticlinal fold structures, i.e. thrust propagation folds, the hinges of which are densely fractured by minor-offset normal faults (Barnes et al. 2010; Wang et al. 2017). Studies of similar structures in outcrops in northwestern China suggest that in such structures the folding is the primary control over fracture distribution, with the fault itself acting as a secondary control (Li et al. 2018). Across these anticlinal folds, fractures primarily develop in two distinct zones; an extensional zone through the fold hinge—with the highest fracture density—and through a

broader area of shortening across the fold with moderate fracture density (Li et al. 2018).

Faults are three-dimensional, heterogeneous, anisotropic, internally complex volumetric zones comprising a variety of internal structures with inconsistent strain distribution across a range of scales (Childs et al. 2009; Manzocchi et al. 2011; Choi et al. 2016). Characterising such systems requires the reconciliation of observations representing either large spatial scales and short temporal scales, or vice versa (Townend et al. 2017). Fault gouge sediments found at the core of the fault are generally low permeability, but may be surrounded by an area of highly permeable fractured sediments that comprise the fault damage zone (Fig. 1) (Wibberley and Shimamoto 2003; Mitchell and Faulkner 2009; Childs et al. 2009; Townend et al. 2017; Li et al. 2018). In a simplistic two-component model with a fault core and a damage zone, the damage zone is defined as the volume of deformed wall rock surrounding the fault surface where fracture density is higher than background values due to initiation, propagation and build-up of slip along faults (Childs et al. 2009; Peacock et al. 2017). Faults in siliciclastic rocks that are resolvable by seismic reflection data are generally surrounded by complex damage zones containing small faults perpendicular to the fault plane and deformation structures, with densities of up to 600 sub-seismic scale faults per 100 m, up to 150 m away from the fault core (Fisher et al. 2001; Torabi and Berg 2011).

Several questions remain regarding the role that faults play in fluid migration and the formation of gas hydrates. Previous studies have observed that the interaction between faults and dipping strata is a primary factor in determining

**Fig. 1** Schematic diagram of fluid flow processes associated with a deep-seated thrust fault and the surrounding damage zone. Inset: focused flow along the underside of the fault core, and/or through the damage zone results in concentrated hydrate formation in dipping strata

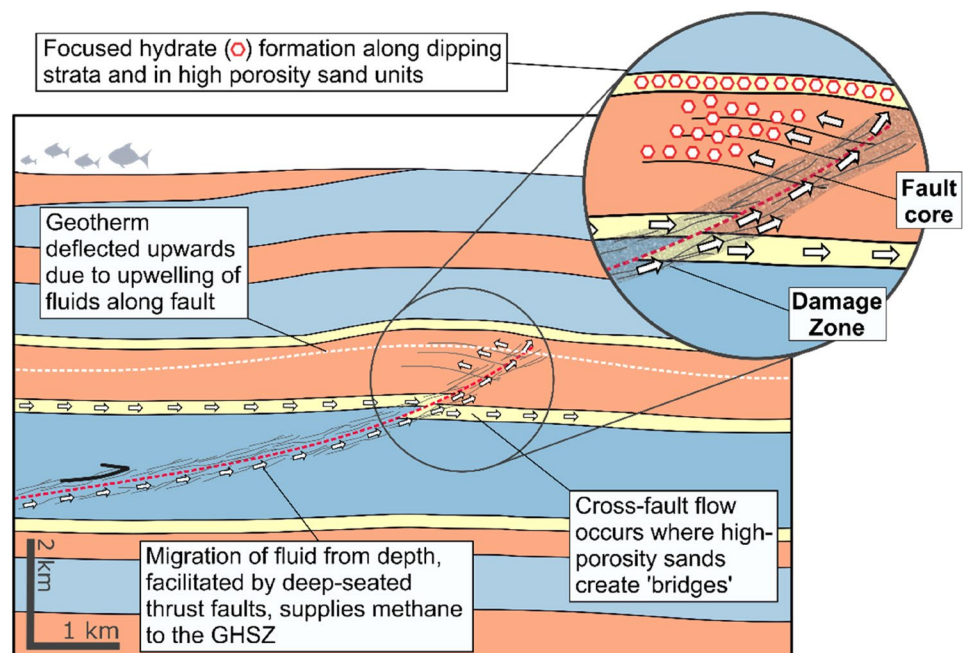
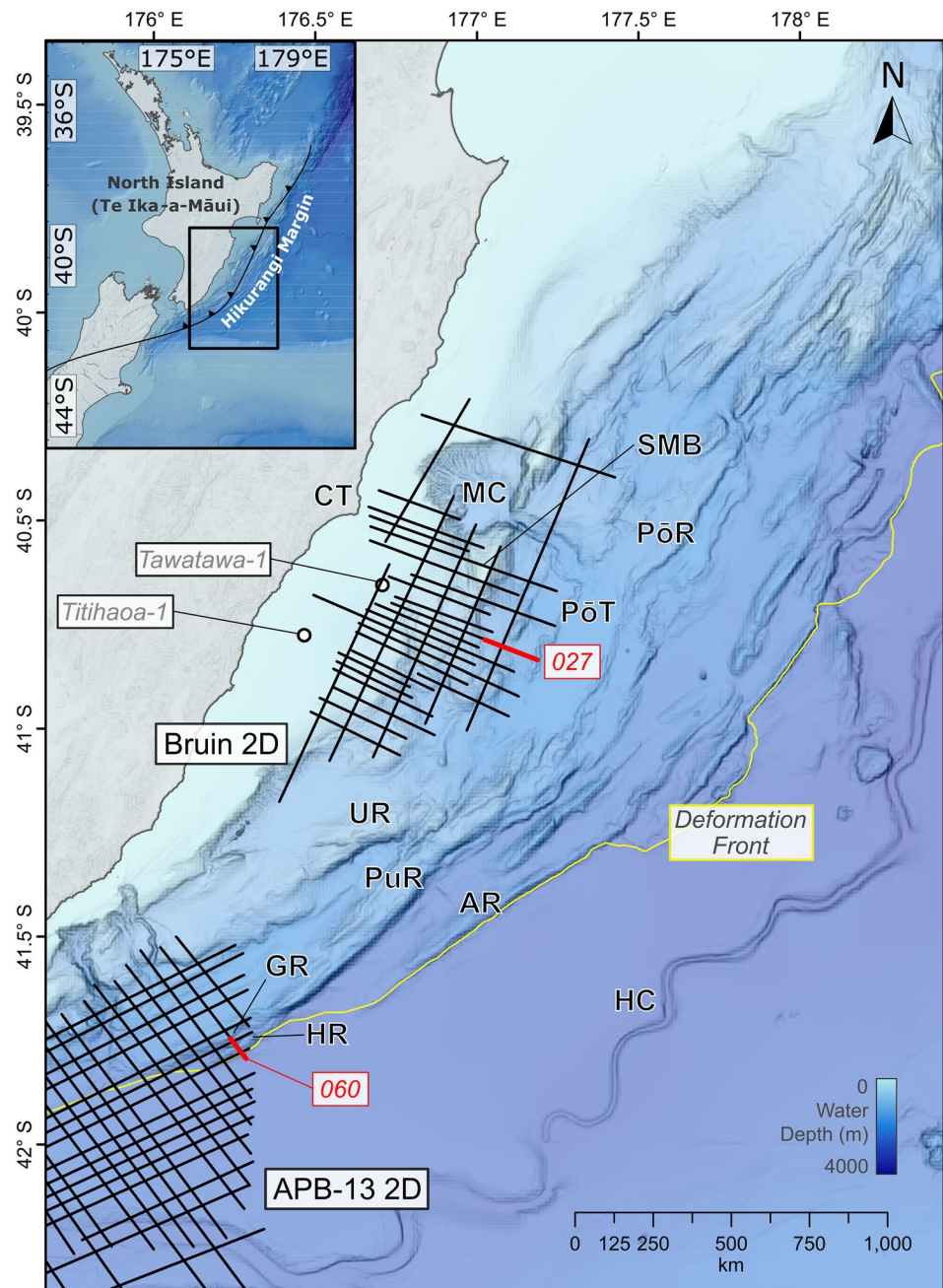


**Fig. 2** Location of the two seismic surveys used in this study. The locations of the two seismic lines used to construct the models are highlighted in red. *AR* Aorangi Ridge, *CT* Cape Turnagain, *HC* Hikurangi Channel, *HR* Honeycomb Ridge, *GR* Glendhu Ridge, *MC* Madden Canyon, *PōR* Pōrangahau Ridge, *PōT* Pōrangahau Trough, *PuR* Pukeroro Ridge, *SMB* South Madden Bank, *UR* Uruti Ridge. Inset map: location offshore the east coast of North Island (Te Ika-a-Māui) with approximate position of the plate boundary indicated by black line. Bathymetry data courtesy of NIWA (Mitchell et al. 2012)



the location of hydrate accumulations (e.g., Wang et al. 2017). In addition, faults may act as ‘bridging’ conduits to allow flow between reservoir sand units that are interbedded with impermeable mud units. In the Gulf of Mexico, interbedded muds and sands have been interpreted as source and reservoir pairs, with the organic rich mud units acting as a source through the production of biogenic methane, and the sand units as reservoirs due to the preferential accumulation of hydrate in coarse-grained units (Cook and Malinverno 2013; Hillman et al. 2017; Nole et al. 2017). However, deeper, and thicker reservoir sand units are thought

to contain hydrate that is primarily sourced from thermogenic sources at depth (You and Flemings 2018). In settings where faults penetrate sufficiently deep into thermogenic gas accumulations, fluid migration along faults could result in mixed gas sources (biogenic and thermogenic) contributing to hydrate formation.

Some uncertainty remains regarding the evolution of fault zone permeability over time, and the impacts this would have on the processes of fluid migration and hydrate formation. The damage zone surrounding the fault core would initially be relatively permeable in contrast to the surrounding



country rock, even if the fault core itself is impermeable. However, over time, with the formation of hydrate, it may be possible for the permeability of the damage zone to decrease as the fractures become ‘sealed’ as hydrate saturation increases (Macelloni et al. 2015). If so, it may be that there are several stages to the development and evolution of fault zone permeability over time, with an initial phase of increased permeability as deformation occurs, with permeability then decreasing in an inverse correlation with hydrate formation. Due to the long timescales involved in fault development, sediment deposition and hydrate formation, it is difficult to constrain and disentangle these processes.

There is also some debate as to whether gas accumulation in anticlinal structures formed by thrust faults—such as those along the Hikurangi Margin—may play a role in contributing to the activation of normal faults. Sets of normal faults with minor offsets are commonly observed at the crests of anticlines and are generally thought to form as a result of localised flexural extension (e.g., Weinberger and Brown 2006). However, there may be a component of pressure-driven fault reactivation (Flemings et al. 2003; Hornbach et al. 2004) due to the accumulation of gas beneath the GHSZ or beneath other low permeability barriers. Examples of this process have been documented from the Hikurangi margin, where gas is channelled upwards into anticlinal folds/ridges via more permeable strata—with or without the aid of the fault itself acting as a flow conduit (Crutchley et al. 2010). Even if the gas plays no part in fault activation, the accumulation of gas may result in dilation of fractures that may be present in the damage zone around existing normal fault structures and a general increase in fracture density.

In this study we briefly discuss the nature of faulting in the southern Hikurangi Margin, before focusing on two examples of locations where thrust faults interact with the gas hydrate system. To do this we use 2D models constructed in the petroleum systems modelling software, Petromod™ (Kroeger et al. 2015; Piñero et al. 2016), using inputs from 2D seismic data along the Hikurangi Margin to investigate the impact of fault properties on fluid migration and hydrate formation. The first of these is based on a 2D seismic line from the Bruin 05 survey near Madden Canyon (Fig. 2) and uses realistic geometries to model a series of low-offset thrust faults that terminate below the GHSZ. The second is loosely based around geometries from a 2D seismic line in the Pegasus Basin APB-13 survey (Fig. 2) but uses a simplified single thrust fault model to determine the impact of varying physical properties across the fault zone. Modelling the gas hydrate system allows us to reconstruct the thermal and pressure conditions that have controlled hydrate stability throughout basin evolution. The generation of thermogenic and biogenic gas is integrated with gas migration and hydrate formation, allowing us to test the influence of geometric faults as fluid flow pathways. Improving the

understanding of factors that control the supply of gas to the GHSZ and the formation of gas hydrates will ultimately enable a better assessment of the distribution of reserves and the effectiveness of potential production mechanisms.

## Geological setting

Subduction along the Hikurangi Margin has been active since ~25 Ma (Walcott 1978; Lewis and Pettinga 1993; McArthur et al. 2019). The margin consists of a ~150 km wide thrust imbricated frontal wedge, with a Torlesse Composite Terrane metasedimentary basement backstop (Barnes et al. 2010; Bland et al. 2015). The frontal wedge is made up of three units, all of which are deforming as a single unit. The first of these is an inner foundation of Late Cretaceous and Paleogene rocks that were deposited prior to the initiation of subduction along the margin, the second is an outer wedge of late Cenozoic accreted trench-fill turbidites; and lastly, a deforming cover sequence of Miocene to Recent shelf and slope basin sediments (Barnes et al. 2010). These sediments are up to several kilometres thick beneath the upper margin and generally thin seawards over the frontal accretionary wedge (Barnes et al. 2010; Bailleul et al. 2013; McArthur et al. 2019). The frontal wedge is characterised by deep-reaching, crustal scale, seaward verging faults that extend from the subduction interface to around the depth of the GHSZ (Barnes et al. 2010; Crutchley et al. 2015). The thrust system forms the furthest seaward expression of deformation in the wedge, with deep-seated thrust faults resulting in the formation of a series of anticlinal ridges and steeply dipping strata (Crutchley et al. 2015; Wang et al. 2017). Many of the ridges along the margin are further deformed by minor normal faults and backthrusts at their crests (Wang et al. 2017). Sedimentation rates along the margin are highly variable, with low sediment input and erosion along the thrust ridges, and high sedimentation in the basins that lie between the ridges and in the trench seaward of the ridges (Henrys et al. 2003).

Subduction systems such as the Hikurangi, with thick trench sequences, have dynamic fluid systems due to dewatering in response to compaction and contractional deformation (Barnes et al. 2010; Johnson et al. 2015). Water saturated trench sediments transition from a gravitational load dominated system at the deformation front, to one where the principle compressive stress approaches horizontal within the accretionary wedge (Barnes et al. 2010). This produces structural permeability which facilitates lateral fluid flow. Previous gas hydrate models have suggested that the formation of concentrated hydrate deposits relies significantly on focused migration of microbial methane, thermogenic natural gas, or a combination of both, often as a free gas phase through interconnected permeable strata, faults and fracture zones (Kroeger et al. 2015, 2019; Fujii

et al. 2016; Crutchley et al. 2017). Such focused migration of gas is considered to be a key process leading to the formation of potential economically viable hydrate accumulations (Liu and Flemings 2006, 2007; Boswell et al. 2012; You et al. 2015).

BSRs are widespread across the Hikurangi Margin, and have been mapped across > 40,000 km<sup>2</sup>, with a broad correlation between the occurrence of high-amplitude BSRs and the location of thrust ridges (Henrys et al. 2003; Crutchley et al. 2015). There is a distinct lack of BSRs in the basin fill between these ridges, and where they are present they are much lower in amplitude relative to those on the ridges (Crutchley et al. 2015). Deep seismic imaging of fluid migration pathways along the Hikurangi Margin suggests that some of the gas that contributes to hydrate formation could be thermogenic in origin (Plaza-Faverola et al. 2012). The most probable source units in the region are marine shales of the Late Paleocene Waipawa and the Late Cretaceous Whangai Formation and Early Cretaceous units (Uruski 2010; Bland et al. 2015). In this study we focus on two areas along the southern Hikurangi Margin; firstly, Madden Canyon and Pōrangahau Ridge offshore Cape Turnagain, and secondly, Honeycomb Ridge in the northern Pegasus Basin (Fig. 2).

### South Madden Bank to Pōrangahau Trough

Model I is based on seismic line Bruin 027 (Fig. 2), located south of Madden Canyon, between South Madden Bank and Pōrangahau Trough, inboard of Pōrangahau Ridge. The seaward edge of the Cretaceous to Palaeogene sequence is thought to be located beneath Pōrangahau Ridge, with the decollement at a depth of ~ 5 km (Pecher et al. 2010; Barnes et al. 2010). Pōrangahau Trough is infilled by a continuous, relatively undeformed sedimentary succession, with folded strata towards the ridges associated with inactive thrust faults (Fig. 3a, c). The BSR is well defined and continuous across much of the basin infill; however, it is patchy and disrupted through the adjacent ridges. Short sediment cores recovered from Madden Canyon and Pōrangahau Trough contained interbedded massive silts and silty sands, with coarser sediments found in the canyon (McKeown 2018). High reflectivity zones imaged in the sediments beneath the ridge have been interpreted as accumulations of free gas.

### Honeycomb and Glendhu Ridges

Slightly further south along the margin from Pōrangahau Ridge there are two parallel NE striking thrust ridges lying in water depths of 1800–2700 m; Honeycomb and Glendhu

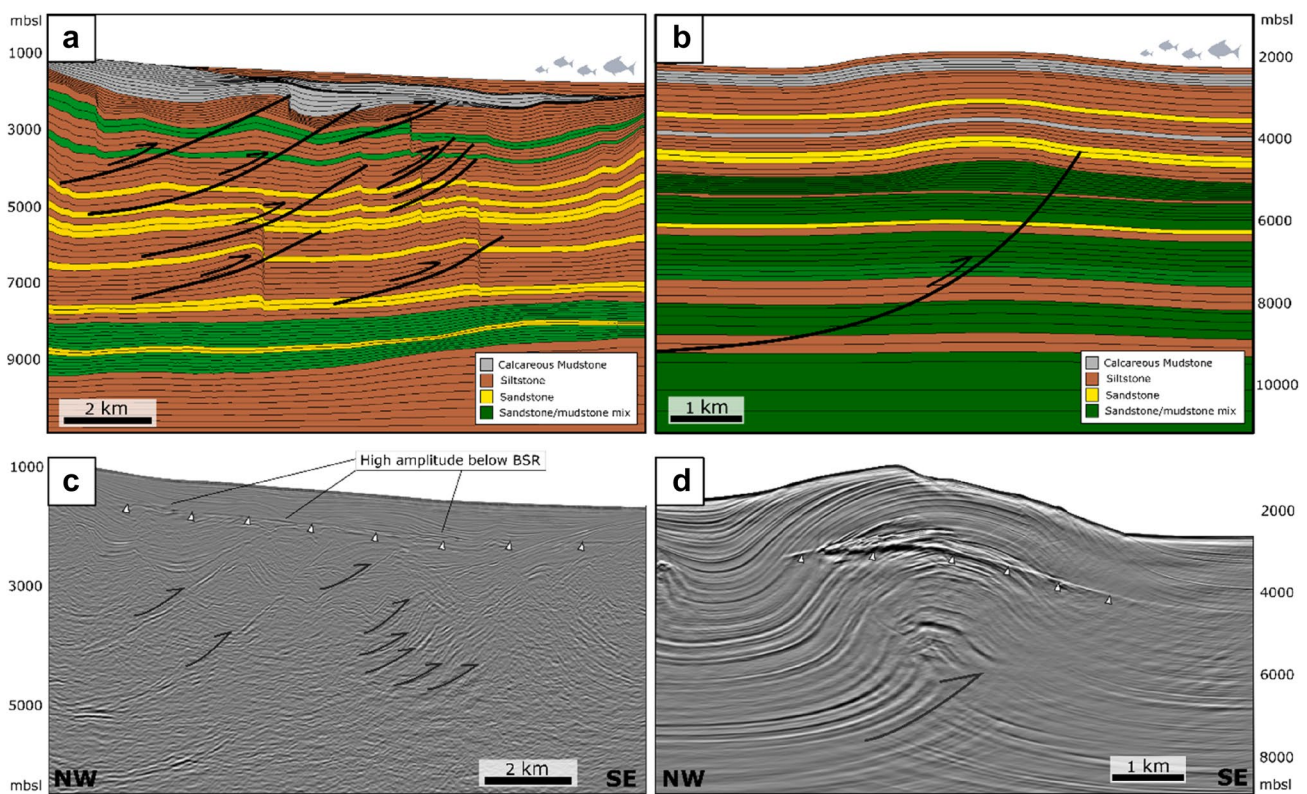


**Fig. 3** Petromod inputs for the two models. **a** Model I—based on the 2D line Bruin 027. **b** Model II—base on the 2D line APB-13-060. Solid black lines indicate the position of thrust faults. **c** Bruin 027 seismic line. **d** APB-13-060 seismic line. See Fig. 2 for line locations

(Barnes et al. 2010; McArthur et al. 2019). The ridges are separated by basins infilled by diachronous sedimentary sequences up to 2500 ms in thickness. Honeycomb Ridge, the site of Model II, and Glendhu Ridge lie immediately inboard of the deformation front, and are traversed by the 2D seismic lines of the Pegasus Basin (APB13) survey. The BSR is well defined as a high-amplitude reflection through the anticlinal ridges but is weak or absent through the small trough that separates Glendhu and Honeycomb Ridges. Landward of Glendhu Ridge the BSR is clearly imaged as a phase reversed reflection; however, its amplitude varies and is not entirely continuous across the basin. High velocity zones above the base of gas hydrate stability (BGHS) here have been interpreted as hydrate bearing sediments, while corresponding low velocity zones are indicative of free gas that is present both above and below the BGHS (Crutchley et al. 2015). Normal polarity, high-amplitude strata are interpreted as gas hydrate bearing, porous sediments. Crutchley et al. (2015) observe a correlation between the position of thrust faults, dipping strata and velocity anomalies that suggests both the faults and dipping strata facilitate gas migration. Penetrating thrust faults that terminate above the BGHS allow free gas to bypass the hydrate bearing sediments, forming free gas accumulations within the GHSZ (Crutchley et al. 2015).

## Data and methods

### Seismic data

Seismic data from two 2D surveys were used in this study (Fig. 3). The Bruin 2D multichannel seismic survey was acquired by Multiwave Geophysical in 2006 with a 4140 in<sup>3</sup> Bolt airgun array towed at a depth of 6 m, and an 8100-m streamer towed at 7 m depth. The streamer comprised 648 active channels spaced at 12.5 m with a shot interval of 37.5 m (Fugro Seismic Imaging Pty Ltd. 2005; Wang et al. 2017). These data were used for Model I. The second survey used is the APB-13-2D Pegasus Basin survey, acquired by CGG Services for Anadarko New Zealand Ltd. in 2014. These data were acquired with a 3610 in<sup>3</sup> Bolt airgun array towed at a depth of 12 m, and an 8100-m streamer towed at a depth of 18 m. The streamer comprised 648 active channels spaced at 12.5 m with a shot interval of 37.5 m and a record length of 10.5 s (EPI Group 2014). These data were used for Model II.

Wang et al. (2017) reprocessed several lines from the Bruin survey, including Line 027 that we use here. Their processing workflow included removal of non-live traces and noisy shots from the data, a Butterworth filter with corner frequencies of 4, 12, 150 and 200 Hz, an upward shift of 50 ms to correct for a recording delay, a correction

for spherical divergence using a time-squared function and application of a Kirchhoff pre-stack time migration. The APB-13 data were processed using a standard industry processing workflow that included reformatting, 2D geometry assignment, re-sampling with an anti-aliasing filter, spherical divergence and receiver motion corrections, surface related multiple elimination and linear noise attenuation (CGG Services Ltd. 2014). To be able to construct geological models in depth from these surveys, we used a smooth 1D velocity curve based on the 2D pre-stack depth migration velocity model of Plaza-Faverola et al. (2012). Due to the lateral complexity of the geology in the region it is not possible to trace key reflections, and velocity boundaries, between the 2D seismic profiles. Therefore, the best approach was to create this smooth 1D model and then drape it beneath the seafloor of the seismic sections we wanted to depth convert. Above the seafloor we used a constant velocity of 1500 m/s for the water column.

### Modelling the gas hydrate system

In this study we constructed two 2D models using the Schlumberger petroleum systems modelling software (Petromod™ v.2016) to investigate the influence of faults on the development of the GHSZ. Petromod™ uses Sloan's formula to determine the phase kinetics of gas hydrate formation, which is then extended to include the dependency of the dissolution pressure on the salinity (Tishchenko et al. 2005; Sloan and Koh 2008; Piñero et al. 2016), while pressure and temperature dependent methane dissolution and diffusion through the model are calculated according to Duan and Mao (2006). Migration of gas is calculated using two phase Darcy flow, while migration in permeable layers is determined by flow path modelling (Hantschel and Kauer auf 2009). Thermogenic methane generation in the models is determined according to the kinetic function defined by Ungerer (1990). The appended kinetic function for microbial generation is based on Kroeger et al. (2015) and references therein.

To construct the models, we used inputs from the 2D seismic data to map the geometry of the sedimentary units, in addition to data from previous studies including well data (Titihaoa-1 and Tawatawa-1) and core samples (Biros et al. 1995; Tap Oil Ltd. 2004) to assign lithologies and age of units (Fig. 3). Model I (Bruin 027 data) is based on realistic geometries mapped in the 2D seismic data (Fig. 3a), while Model II (APB-13-060 data) is loosely based on the geometry of the units mapped in the 2D seismic data (Fig. 3b). The geometry of the units in Model II has been simplified to test scenarios with variable fault properties. This allows us to focus specifically on the properties of the fault by eliminating the complexity of the sedimentary strata. A similar approach has been employed when investigating complex



gas hydrate systems elsewhere, such as the Gulf of Mexico (Chatterjee et al. 2014; Nole et al. 2016) whereby the system is broken down into manageable pieces, isolating the component to be tested. It is well established in computational modelling that models with fewer moving parts are easier to grasp, allowing us to more clearly connect cause and effect (Paola and Leeder 2011). Even if they do not precisely replicate the 'real-world' systems, simplified models can serve as valuable reference cases (Power et al. 1998).

The sub-surface strata are imaged relatively clearly to ~5000 ms beneath the seafloor, with some isolated deeper structures imaged down to ~8000 ms. Due to the limited imaging of deeper structures in the 2D seismic data, other seismic lines from the region were used to construct the lower portion (>7000 m) of the models. Lateral resolution across both models is set as a 5 m grid, with vertical resolution of the grid defined by layer thickness, which varies from 5 to 250 m for Model I, and 5–650 m for Model II. Due to the lack of well control, some assumptions must be made with regard to the characteristics of the sedimentary sequence in both models. As such, a simplified sequence is used, with the lithology assigned based on regional data. A sensitivity analysis was conducted to determine which parameters had the greatest potential to influence the model outputs.

Fault dimensions and physical properties are based on the recently acquired logging-while-drilling (LWD) and core data from IODP Expedition 375, hole U1518 on the northern Hikurangi Margin (Pecher et al. 2018; Saffer et al. 2018). To alter the permeability of the fault between the two end members (open and closed), different shale gouge ratio values were assigned to the faults. Shale gouge ratio (SGR) can be defined as an estimate of the proportion of fine-grained material entrained into the fault gouge from the surrounding host rocks (Yielding et al. 1997). Faults are represented using locally refined volumetrics, where migration occurs via percolation along the cell boundaries, but also incorporates a locally refined grid along the fault to calculate the influence of the faults on pressure. Due to limitations in constraining the timing of fault activity in the region, we focus on the present-day geometry and state of the GHSZ. Two parameters are kept constant across all models; heat-flow ( $46 \text{ mW/m}^2$ ) and sediment water interface temperature ( $2 \text{ }^\circ\text{C}$ ). These values were based on testing of the models using published values from the region (Field et al. 1997; Fugro Marine Geoservices 2015; Kroeger et al. 2019). The models were run with a range of heatflow values from published data, allowing us to constrain the value that provided the best fit between the modelled base of gas hydrate stability, and the observed position of the BSR in the seismic data in Model I.

The models were tested with both open and closed basin sides, this parameter has limited influence on hydrate generation, but closed sided models tended to result in

anomalously large fluid flow vectors across the basin. As a result, all models are run with open basin sides for the purposes of this study.

## Results

### Faulting in the southern Hikurangi Margin

There are numerous examples in seismic data along the Southern Hikurangi Margin of faults interacting with BSRs and other indicators of hydrates and free gas (Fig. 4). Both thrust faults and normal faults are abundant along the Hikurangi Margin, and frequently coincide with high-amplitude bright spots beneath the BSR where they intersect or approach the BGHS. There are several examples of deep-seated thrust faults related to anticlinal ridges along the margin that are associated with abrupt terminations of high-amplitude reflections along the fault trace (e.g., Fig. 4e). These high-amplitude strata are interpreted as higher permeability gas-bearing sediments. This indicates that in such settings, these faults are effectively impermeable to gas and do not permit cross-fault flow, therefore restricting free gas to one side of the fault. However; this is not always the case, in some settings high-amplitude strata are clearly continuous across faults (e.g., Fig. 4b). The examples in Fig. 4 highlight the variability in the styles of faulting and lithological styles across the Hikurangi Margin.

High-amplitude strata above the BSR are often indicative of concentrated gas hydrate deposits within the GHSZ. Along the southern Hikurangi Margin such features are commonly observed in the limbs of anticlinal folds in the hanging wall of deep-seated thrust faults (Fig. 4a and c), as also documented by (Crutchley et al. 2019). Similarly, high amplitudes immediately beneath the BSR are frequently observed in anticlinal folds (Fig. 4c), both with/without overlying high-amplitude strata in the GHSZ.

### Sensitivity Analysis

Due to the lack of data available to directly calibrate the models, there is a significant degree of uncertainty in the results. In order to determine the impact of fluctuations in parameters on the model outputs we conducted a sensitivity analysis (Balaman 2019). The sensitivity analysis allows us to identify high-leverage variables, whose values have a significant impact on the modelled system, and low-leverage variables, whose values have minimal impact (Jørgensen and Fath 2011). We use a simple approach to test the sensitivity of the model to variations in parameters. To do this, we increased one parameter value by 10% or 50% and examined the change in average gas hydrate saturation in the area

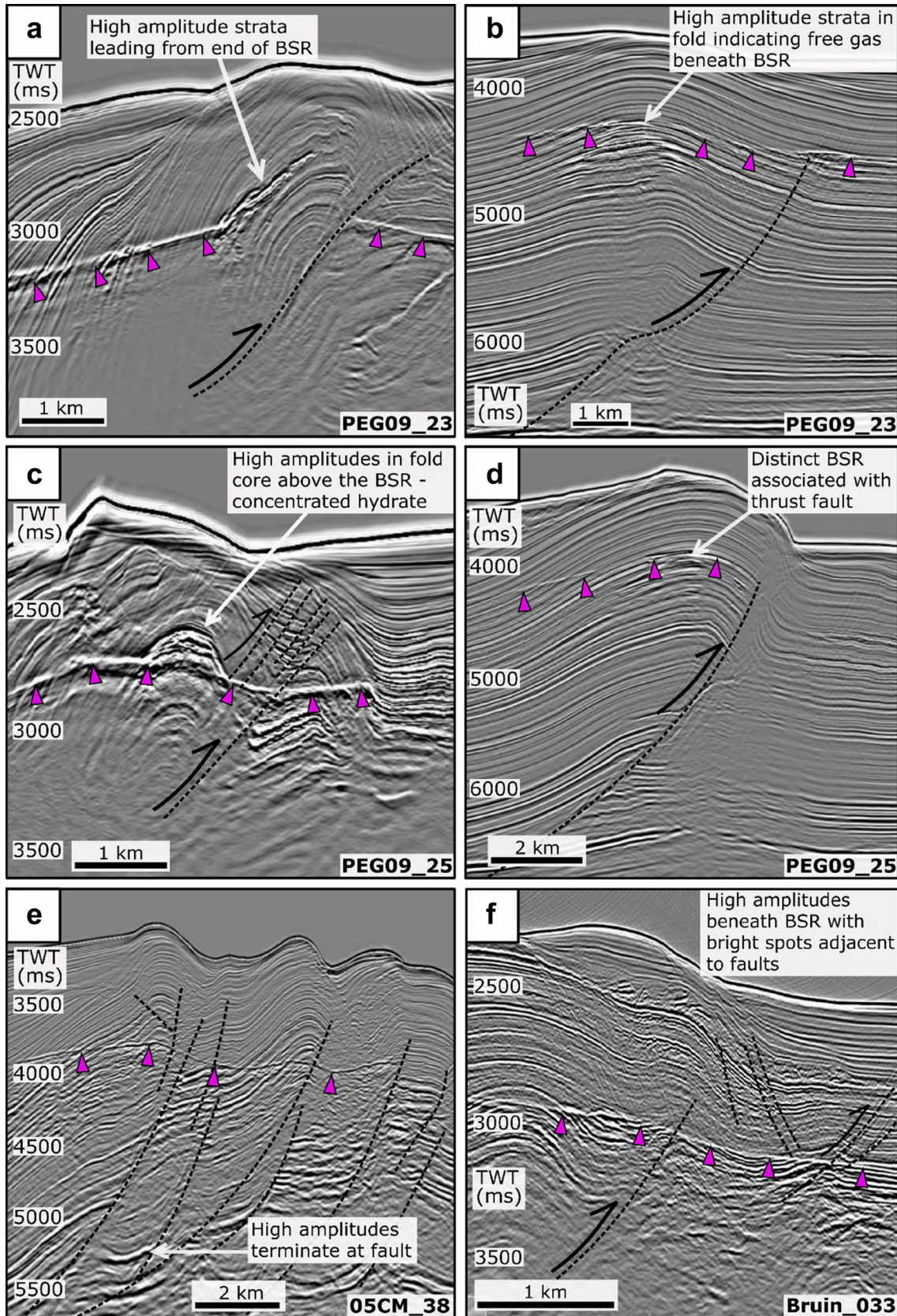




**Fig. 4** Examples of the relationship between faulting and hydrates along the Southern Hikurangi Margin. Pink triangles = BSR, black dashed lines = faults. **a** Distinct BSR broken at a large thrust fault along Pukeroro Ridge with a high-amplitude ‘finger’ leading from the termination of the BSR. **b** Bright spot in strata through the core of a fold with chaotic seismic facies leading up from a deeper thrust fault. **c** Distinct high amplitudes through the core of a thrust-related fold. **d** and **e** High-amplitude strata terminate abruptly at thrust faults at depth with overlying bright strata beneath the BSR. **f** High amplitudes immediately underlying the BSR with bright spots adjacent to fault traces

between the seafloor and the BGHS in the model. The results of the sensitivity analysis are summarised in Table 1.

As would be expected, larger variations in parameters have a greater impact on the average gas hydrate saturation. The exception is that a 50% increase in the heatflow (an increase from 46 to 69 mW/m<sup>2</sup>) actually reduces the average gas hydrate saturation. This is due to the fact that such an increase in the heatflow significantly shifts the position of the base of the gas hydrate stability zone towards the seafloor, and therefore decreases the average gas hydrate saturation in the model. As the aim of this study is to investigate the impact of variations in fault properties, the porosity and lithology of the units are kept constant across the models to ensure that the observed changes are not influenced by changes in the lithology.

In addition, we tested the model by varying heatflow over time within the range of published values from the region (42–50 mW/m<sup>2</sup>) to determine the impact of constant vs. variable heatflow (Field et al. 1997; Fugro Marine Geoservices 2015; Kroeger et al. 2019). This resulted in only a 1.89% increase in average gas hydrate saturation, indicating that this would not have a significant impact. Therefore, to avoid over-complicating the model we have kept heatflow constant throughout.

## Model I

Model I is located south of Madden Canyon, slightly inboard of the southern extension of Pōrangahau Ridge. This area is characterised by a series of small ridges associated with blind thrust faults. A series of minor offset, blind thrust faults can be mapped across the line, resulting in the formation of several small anticlinal structures to the NW of the faults. Fluid flow through conduits such as faults brings fluid up from depth which may then be channelled laterally along high-permeability, commonly sand-rich, layers. These layers allow the fluids to spread out within the GHSZ. Faults and fractures beneath the ridge axis generate secondary permeability that may allow fluids to breach the BGHS and extend into the GHSZ. Finally, folded high-permeability, sand-rich,

strata that cross-cut the BGHS provide a transport mechanism for fluids into the GHSZ from depth.

In order to constrain the end-member conditions for the models, both were initially run with the faults entirely open as fluid flow conduits, and then entirely closed to fluid flow (Table 2) (Yielding et al. 1997). This allows us to establish a starting point for determining the properties of the faults in each model. Petromod™ deals with faults as geometric features, not tectonic activities, hence the characteristics assigned to the faults in the model determine how the simulator handles the impact of faults on fluid flow.

When Model I is run with the faults open to fluid flow (Ia, Table 2) the predicted position of the BGHS is generally coincident with the mapped position of the BSR in the seismic data when using a heatflow value of 46 mW/m<sup>2</sup> (Fig. 5a). As shown in Fig. 5, the position of the BGHS does not change significantly in the different model scenarios. Hydrate distribution across the model is heterogeneous, with highly-saturated patches located above the termination of the two shallowest thrust faults (Fig. 5a). This distribution is consistent with the variation in amplitude of the BSR across the 2D seismic line (Figs. 3c and 5). At the other extreme, running the model with the faults closed (Ib) to fluid flow results in very limited hydrate generation, producing 69.23 Mton less gas hydrate (Fig. 5). As a control, the model was also run with the same sediment geometry, but with the faults removed (Ic). This resulted in increased hydrate accumulation relative to Model Ib (27.34 Mton more), but less than that generated in Model Ia (41.89 Mton less) when the faults were open to fluid flow. This further supports the concept that the faults act as fluid migration conduits for the formation of highly-saturated hydrate deposits.

Varying the permeability of the fault zone using shale gouge ratio (SGR) values further reinforces that the faults are primary fluid flow pathways. SGR values of 35% (Id) and 70% (Ie) were used to represent high and low permeability faults, respectively. The distribution of hydrate produced in these two scenarios is similar to that of Model Ia; however, as expected the levels of gas hydrate saturation increase in correlation with increased permeability (Fig. 5d and e). Model Id (35% SGR) produced 76.77 Mton of gas hydrate, whereas Ie produced 53.86 Mton in total. In addition, with reduced permeability (Ie) the distribution of hydrate in the model result is restricted to the apex of the anticlinal folds and focused just above the BGHS with no hydrate produced in the unit immediately beneath the seafloor.

Fluid flow vectors in Model Ia suggest that multiple fluid flow pathways are active at different depths beneath the seafloor (Fig. 6a). Focused flow along faults and strata is more apparent at depth, with vertical fluid flow (across layering) becoming more pervasive at shallower depths where there is lower effective stress due to the increasing permeability contrast between the fault rock and surrounding sediment

**Table 1** Results of a +10% and +50% sensitivity analysis (GH<sub>sat</sub> = average gas hydrate saturation)

	+10%	+50%
	Change GH <sub>sat</sub>	Change GH <sub>sat</sub>
Porosity of lithology (shallow)	0.06	0.87
Porosity of lithology (deep)	0.36	0.64
Heatflow	0.75	-0.02
Sediment–water interface temp	0.42	0.81

**Table 2** Summary of fault parameters used in models

Model no.	Fault architecture	Fault properties
Model I-a	Planar	Open to fluid flow
Model I-b	Planar	Closed to fluid flow
Model I-c	–	Faults removed
Model I-d	Planar	35% SGR
Model I-e	Planar	70% SGR
Model II-a	Planar	Open to fluid flow
Model II-b	Planar	Closed to fluid flow
Model II-c	–	Faults removed
Model II-d	Planar	35% SGR
Model II-e	Planar	70% SGR
Model II-f	Strata—3 layers	Open core, closed fracture zone
Model II-g	Strata—3 layers	Closed core, open fracture zone

SGR shale gouge ratio

with depth, due to compaction. Vertical flow appears to be focused above the shallower terminations of the blind thrust faults when the faults are open to fluid flow (Fig. 6a). Where the faults are closed to fluid flow the flow vectors are restricted to along strata flow with limited flow around the fault terminations; however, there is substantial vertical flow in the shallow section of the model (Fig. 6b).

As with previous models (Kroeger et al. 2019), our results suggest that shallow biogenic generation of methane is the primary source for hydrate formation (Fig. 6). However, the influence of introducing or removing faults on hydrate accumulation suggests that faults may also play a role in supplying methane from deeper, likely thermogenic sources. Although as these deep faults also tap into the shallower biogenic gas source they would provide additional conduits for focused flow of shallow sub-BSR gas into the GHSZ, even in the absence of deeper thermogenic gas.

## Model II

Model II is generally based on a 2D seismic line from the basin-wide APB-13 2D seismic survey. This line transects Honeycomb Ridge, an accretionary ridge that lies immediately landward of the deformation front. For the purposes

of the model, the sediment and fault geometries have been simplified to focus on the structure of one large thrust fault that terminates beneath the ridge. This allows us to manipulate the fault and test several different fluid flow scenarios, creating a conceptual model that would be applicable to other accretionary ridge structures along the southern Hikurangi Margin such as Aorangi and Pukeroro, and also relevant to other hydrate provinces in subduction margins. In Model II we tested several scenarios to determine the impact of extending the fault tip upwards, with the termination occurring immediately below, or extending into, the GHSZ. These scenarios were all run with the fault open to fluid flow (IIa). The results of these tests clearly show notably increased hydrate accumulation as the fault termination extends towards the seafloor (Fig. 7). This also shows increased hydrate formation away from the anticline, which reflects the enhanced influence of the fault when it terminates closer to the BGHS (Fig. 7c).

As with Model I, Model II was initially run in the two end-member states of faults open to fluid flow (IIa) and closed to fluid flow (IIb). Model IIb produced slightly less hydrate than IIa (6.62 Mton less), suggesting that, as with Model I, the faults are required as a migration pathway to supply gas to the GHSZ. Model II was initially run with the fault terminating at a greater depth, as the fault is not clearly imaged in the shallow section. However, this model produced a limited amount of gas hydrate across all fault scenarios, which is inconsistent with the imaging of a high-amplitude, distinct BSR in the seismic data. The fault was then extended upwards in the model, without changing the overall geometry of the strata, terminating 2500 m below the BSR (Fig. 8). This resulted in a substantial increase in the volume of hydrate produced, further reinforcing that the fault is critical to facilitating the upward migration of gas into the GHSZ.

Closing the fault in Model II to fluid flow (IIb) slightly reduced the amount of hydrate formed relative to the fault being open to flow (IIa). However, there is a distinct change in the lateral distribution and vertical extent of hydrate saturation in the model result (Fig. 8a and b). Both of these models show a clustered distribution of hydrate around the apex of the anticlinal fold at the centre of the line, with an increased spread in hydrate towards the shallower sediments in IIa, where the fault is open to fluid flow. Flow vector patterns across the two end-member models (IIa and IIb) are relatively similar, aside from the fault flow vectors being present in IIa that are of course absent in IIb (Fig. 9). As in Model I, the generation of methane is focused immediately beneath the BGHS. Model IIb, run with the fault closed to fluid flow, clearly shows the accumulation of gas against the fault surface (Fig. 8h), showing a similar result to that observed in the seismic data (Fig. 4e), where high-amplitude strata abruptly terminate against a fault surface.



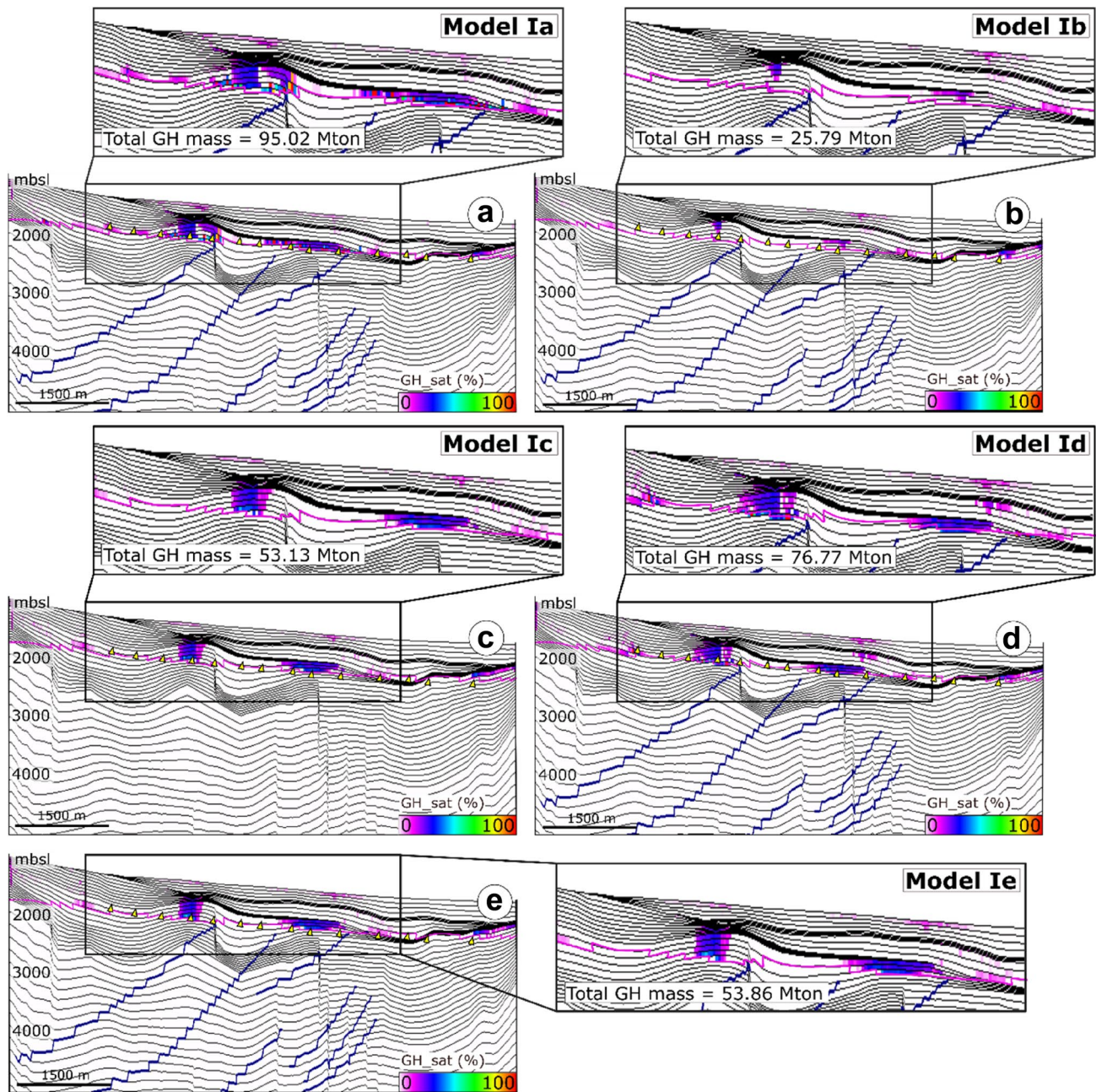


**Fig. 5** Model I: 2D model results showing gas hydrate saturation under variable fault conditions. Dark blue lines = fault locations, pink line = modelled BGHS, yellow arrows = mapped BSR from seismic

line. **a** Faults open to flow; **b** faults closed to flow; **c** faults removed; **d** semi-permeable faults with SGR ratio of 35%; **e** reduced permeability faults with SGR ratio of 70%

To confirm the impact of faults on fluid flow the model was run with the faults removed (Fig. 8c). The results show slightly increased gas hydrate saturation relative to Iib (with the faults closed to fluid flow); however, there is a decrease in hydrate saturation and reduced vertical distribution of hydrate, constrained to just above the predicted BGHS, compared to Iia where the faults are open to fluid flow. The total mass of hydrate produced was slightly less than that in Iia (4.23 Mton less); however, this is greater than

that produced where the fault was closed (Iib). Varying the SGR value for the fault from 35% (Iid) to 70% (Iie) results in a slight change in the distribution of hydrate across the model; however, there is only a slight decrease in the overall mass of hydrate formed (3.49 Mton less in Iie) (Fig. 8d and e). In Model IIf and IIg, the fault is modelled as a three-layered package of strata, with the middle layer representing the fault core, and the outer layers the surrounding damage zone. In IIf the fault core is open to flow, while the damage



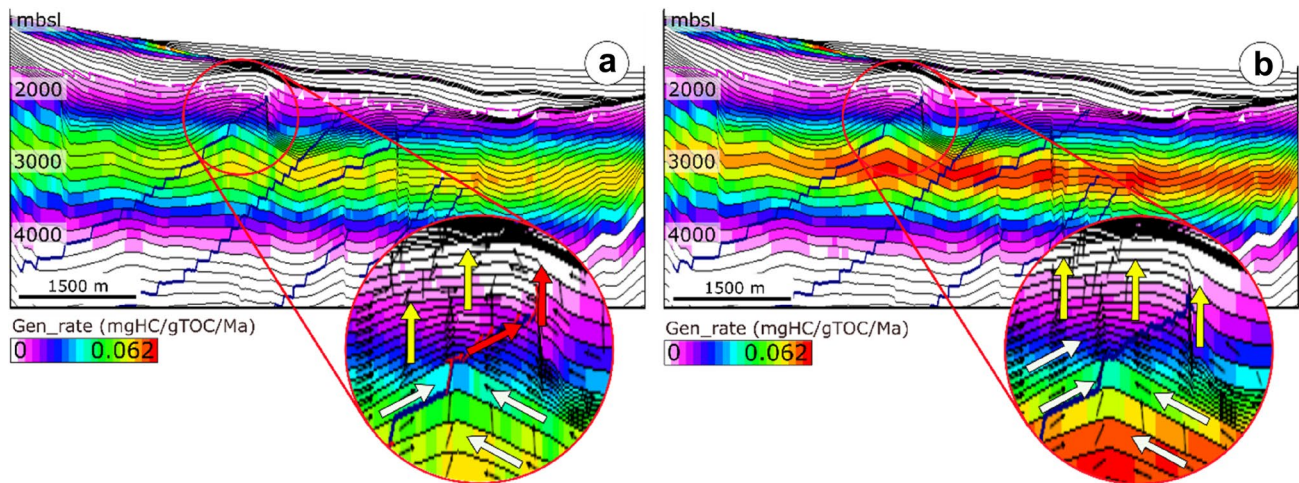


**Fig. 6** Model I: Generation rate of microbial methane per total organic carbon (TOC) mass (Gen\_rate). The generation rate of methane is measured as mass in milligrams (mg) per total mass of organic carbon (gTOC) per million years (Ma). Enlarged sections show over-

laid fluid flow vectors, white arrows=along strata flow, red=fault flow, yellow=vertical flow. **a** Faults open to flow; **b** faults closed to fluid flow

zone is closed, and vice versa in IIg. The results of these two models indicate that both scenarios provide sufficient fluid flow to form a concentrated hydrate deposit in the apex of the fold, however; there is a marked difference in the flow vectors between the two model results (Fig. 9). In Model IIg, where the core is open to fluid flow, there is increased flow along the fault relative to Model II. The total mass of hydrate produced in both these scenarios is similar, 16.47 Mton in IIg and 17.24 Mton in IIg.

## Discussion

### What are the limitations of these models?

Due to the lack of well data available in the region, we must make assumptions regarding the lithological and physical properties of the sediments as we cannot calibrate the model directly. The interpretations used in the models have been based on extensive regional studies (Barnes et al. 2010; Plaza-Faverola et al. 2012; Crutchley et al. 2015), comparisons to onshore analogue outcrops and limited well data that lie outside the gas hydrate stability zone (Biros et al. 1995; Tap Oil Ltd. 2004). In addition, the models are influenced by the resolution of the 2D seismic data that is used to interpret the stratigraphic architecture, and the resolution of the cells in the models themselves. Models are able to address processes at the scale of the model; however, they cannot fully account for the thermodynamic and hydrodynamic effects on hydrate formation at the grain scale of sedimentary rocks (Clenell et al. 1999; Kroeger et al. 2015). It is impossible to

explicitly model all internal complexity of fault zones at the scale of a model; therefore, we use conceptual models that represent those aspects critical to controlling fluid flow at the scale of interest (Manzocchi et al. 2008). In this case, that is at the scale of individual anticlinal ridge structures, where fault zones are the key feature of interest. Petromod™ has been well adapted for the purposes of modelling gas hydrate systems; however, it does have limitations. In spite of this, these models are informative, allowing us to further our understanding of the role that fault zones play in migration of fluids and the formation of gas hydrates in an active subduction margin setting. The results of the sensitivity analysis allow us to identify high-leverage variables (large variation in heatflow and the sediment–water interface temperature) that may have a significant impact on the modelled system. The sensitivity analysis ensures that the observed effects in the model outputs are related to the changes in fault properties, rather than other factors which have a smaller range.

The BSR observed in the seismic data is primarily a manifestation of the presence of free gas in the sediment. When comparing the results of the modelling to observations in the seismic data we can use the amount of hydrate generated, the position of the modelled BGHS and the amount of free gas as indicators of what we might expect to see in terms of amplitude anomalies in the seismic data. However; without ground truth data such as well data it is not possible to quantitatively compare model results to the seismic data as there remains uncertainty in the correlation of seismic amplitudes to gas and hydrate concentration (Holbrook et al. 1996; Hillman et al. 2017). We therefore focus on the implications of variable fault properties on the relative concentration and

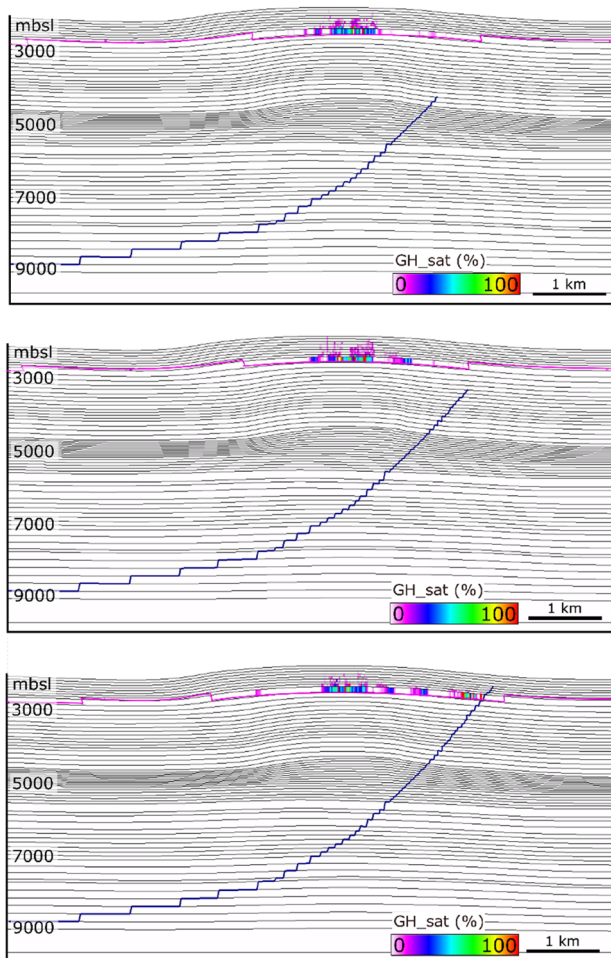


**Fig. 7** Model Iia (open fault) run with variable fault termination depths. The impact of extending the fault upward towards, and into, the GHSZ on hydrate saturation is clearly demonstrated. Pink line indicates the modelled base of gas hydrate stability

distribution of hydrate, rather than drawing conclusions regarding the absolute saturation values. Future research aimed at estimating gas hydrate saturation from anomalous seismic velocities would provide a way of testing our modelling results.

### What is the impact of variable fault properties on fluid flow and hydrate formation?

The impact of fault zones on fluid flow is related to their displacement magnitude and variation in fault rock properties. Faults with a large damage zone will not necessarily have an increased sealing capacity relative to smaller fault complexes (Fisher et al. 2001). Faults can act as permeability barriers or baffles to flow in two ways, through juxtaposition of reservoir rocks or permeable carrier beds onto less permeable, non-reservoir rocks, and the formation of impermeable fault gouge deposits (Manzocchi et al. 2008;

Fisher et al. 2018). Studies of onshore fault systems show that permeability can vary by several orders of magnitude across a relatively short distance (10 s to 100 s of metres) (e.g., Wibberley and Shimamoto 2003). Permeability across fault zones is primarily a factor of secondary damage and fracturing, in contrast to the generally low permeabilities associated with the principal slip surface. The density of such fracturing is related to factors such as lithology, layer thickness, structures such as folds, the position within structures, proximity to thrust faults and the ramp cut-off angle (Li et al. 2018). In addition, fracturing tends to be increasingly well developed in the hanging wall of thrust faults relative to the footwall (Li et al. 2018).

Faults are generally represented as simple planar membranes in fluid flow models, thereby explicitly representing the juxtaposition effects of faulting due to sediment architecture and geometry. We use this approach in Model I and Model Iia-e (Figs. 4, 5, 6, 7). However, the impact of faulting on cross-fault flow where faults act as baffles, and vertical flow between isolated units, is not inherently represented, and the accuracy of these components in fluid flow modelling is inconsistent. In Model IIf and IIg we have attempted to represent some of the complexity that is present around the fault zone, using a layered fault structure to mimic a fault core and the surrounding damage zone (Figs. 6 and 7). The scale at which faults are imaged in seismic data makes it impossible to explicitly represent the internal complexity of fault zones at outcrop scale. Therefore, in order to understand these processes, we rely on simplified conceptual models to highlight the aspects that are critical to fluid flow at the scale of interest. Overall, Model I produced significantly more hydrate in terms of total mass when compared to Model II, likely as a result of the increased area covered in Model I. However; the variations across the different scenarios for each of the models were within a reasonable range. Therefore, it is likely that the difference in mass produced between the two models is a function of the variations in lithology, water depth and overall geometry of the models. Due to the limitations in the models, as discussed, and the lack of ground truth information regarding saturation and/or volume of hydrate present in the region, we place more emphasis on relative variations in hydrate saturation than on absolute values. Relative variations across the modelled scenarios give us insight into the influence of fault properties on the mass of hydrate produced.

Where the fault core and/or damage zone are impermeable to flow, the fault becomes a barrier. Additionally, even if the fault itself is permeable, where a fault juxtaposes permeable strata onto impermeable strata, this may create a localised barrier, preventing along-strata flow. This can be observed in seismic data where high-amplitude strata abruptly terminate against a fault surface (Fig. 4d). In Model I, this is also evident where hydrate accumulation is



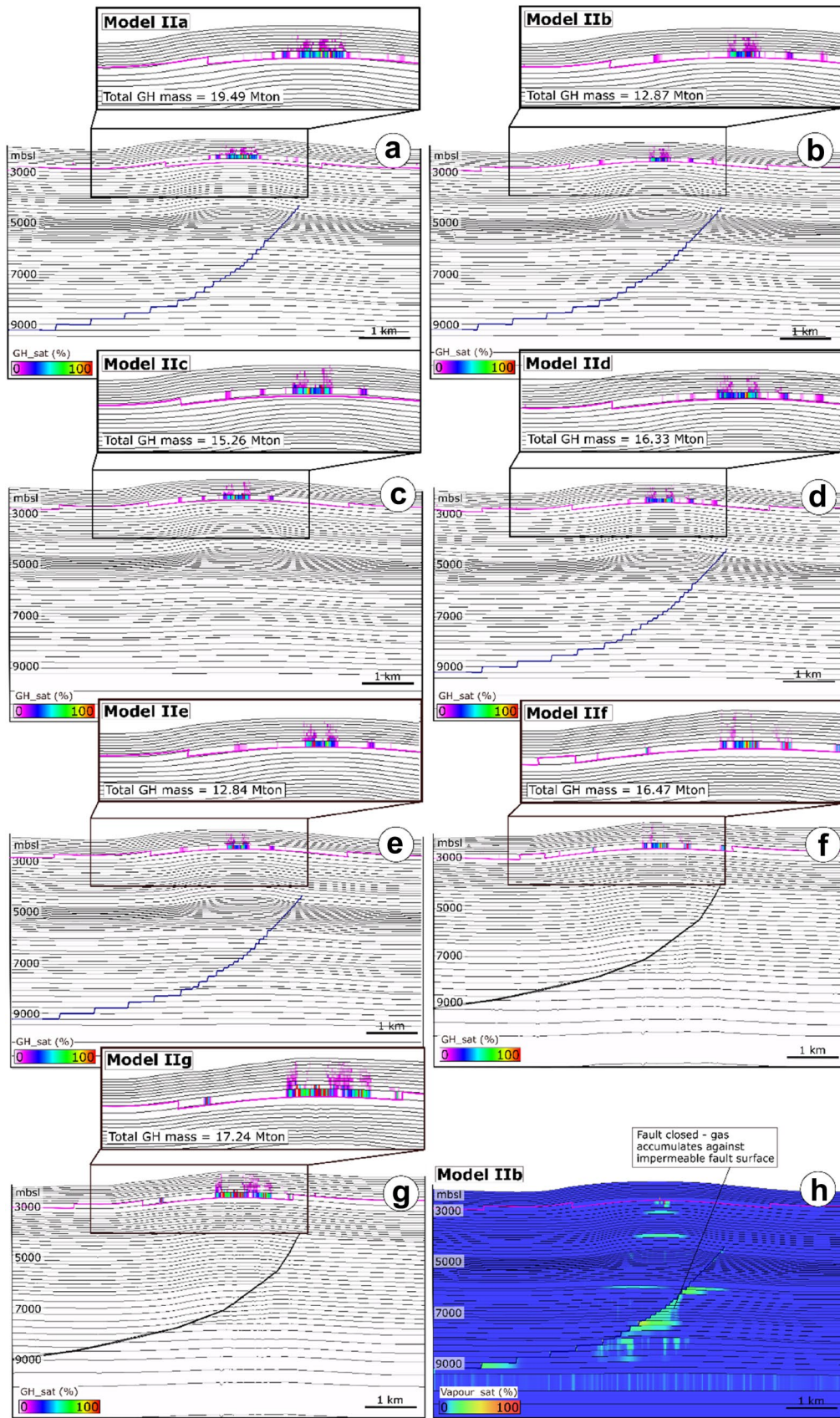




**Fig. 8** Model II: 2D model results showing gas hydrate saturation (GH\_sat) under variable fault conditions. Dark blue lines = fault locations, pink line = modelled BGHS. **a** Fault open to flow; **b** fault closed to flow; **c** fault removed; **d** semi-permeable fault with SGR ratio of 35%; **e** reduced permeability fault with SGR ratio of 70%; **f** 3-layer fault with open core and closed damage zone; **g** 3-layer fault with closed core and open damage zone. **h** Model IIb: abrupt termination of gas saturation against the impermeable fault surface

substantially higher to one side of the shallowest fault terminations (Fig. 5). Model IIb demonstrates nicely the impact of an impermeable fault surface on gas accumulation, with significant build-up of gas against the fault and restricted upward flow into the GHSZ (Fig. 8h). The impact is less apparent in the flow vectors of Model II, although in II f and g there is a distinct pattern in along strata flow vectors which are diverted into the fault in II f, and dissipate into vertical flow in II g. This suggests there is increased fluid flux to one side of the fault; however, this is likely enhanced by the interaction of the fault plane and the geometry of the strata as the folded layers are more steeply dipping to the north-west side of the faults in our models. The results of our models show that in addition to changing hydrate concentration overall, faults may influence fluid flow patterns and thereby shift the areas where the highest hydrate concentrations are to be expected. The exact nature of this relationship depends on highly localised factors such as lithology and physical properties of the sediment; however, this is something that must be taken into account when modelling such systems, particularly if trying to assess the volume of hydrate present.

Faults also play a role in controlling the position of the geotherm as they facilitate the upward migration of warm fluids from depth, which may result in the GHSZ becoming domed above faults (Macelloni et al. 2015; Patterson et al. 2018). Previous work by Henrys et al. (2003), however, suggests that near-surface faults along the Hikurangi Margin only play a secondary role in controlling heatflow anomalies, with topography being the primary influence. Heatflow values along the margin vary with the thickness of the accretionary prism and subducting plate, with values of  $\sim 55$  mW/m<sup>2</sup> at the toe of the prism, decreasing to  $\sim 35$  mW/m<sup>2</sup> 100 km landward of the deformation front (Henrys et al. 2003). Due to the limitations of the 2D modelling, our models only fully account for conductive, not advective heatflow. However, the results show a generally good agreement between the position of the BSR mapped in the seismic data, and that of the modelled BGHS (Fig. 4). This suggests that the geothermal gradient is not considerably perturbed by warm fluid flow along the fault zone at these locations.

## Are faults or folds the primary control on fluid migration?

Our model results demonstrate that extending a thrust fault upwards towards the seafloor strongly impacts the level of hydrate produced (Fig. 7). This suggests that the fault is the primary control over the migration of gas from depth, and that the folded strata associated with the fault merely permit the lateral flow of gas away from the fault zone, focusing hydrate accumulation in the apex of the anticlinal structure. Without the fault extending up to, or near to the BGHS, the folded strata alone would be insufficient migration pathways to result in substantial hydrate accumulation, although we do still see hydrate formation to a lesser extent in II c, in the absence of a fault. This suggests that in a scenario such as Model I, where faults extend to shallow enough depths beneath the GHSZ, faulting becomes the primary controlling factor in the migration of fluid and formation of gas hydrate. However, where faults terminate at greater depths beneath the seafloor, they will have less influence over hydrate formation and the stratigraphic architecture will become key in controlling the distribution of gas hydrate. Our model results demonstrate that reducing the permeability, or closing faults to flow entirely, significantly reduces the amount of hydrate produced (Figs. 5 and 8). Furthermore, altering the characteristics of the fault shifts fluid flow patterns and hence the distribution of hydrate formation. The maximum dip of strata within the GHSZ in Model I is 14°, and 15° in Model II. These dips are relevant in the context of a recent study by Crutchley et al. (2019) who determined that concentrated hydrate formation occurs preferentially in regions where strata dip is  $> 5^\circ$ , and likely  $> 15^\circ$ . Fluid flow vectors in both Models I and II suggest that along strata flow is consistently the dominant flow pattern at depths  $> 2000$  mbsf, unless thrust faults are present to facilitate fluid flux across strata. However, the dominance of along strata flow is only possible where laterally continuous, permeable carrier beds are present, which is strongly dependent on the localised lithological patterns. As discussed by Crutchley et al. (2019), the impact of other factors such as ridge erosion, fore-arc sub-basin sedimentation and gas recycling is likely to become more significant with enhanced ridge topography.

The two models presented here have contrasting geometries, with Model I containing numerous smaller-scale thrust faults, forming a series of narrow anticlinal structures, whereas the solitary thrust fault in Model II forms a broad anticlinal structure. The results of these two contrasting models, particularly when comparing models where the fault properties are consistent (e.g., Model Ia and Model IIa), suggest that as the size of the anticlinal fold increases, the impact of the fault on hydrate accumulation decreases. This indicates that the relative impact of faulting is much more significant in faults associated with

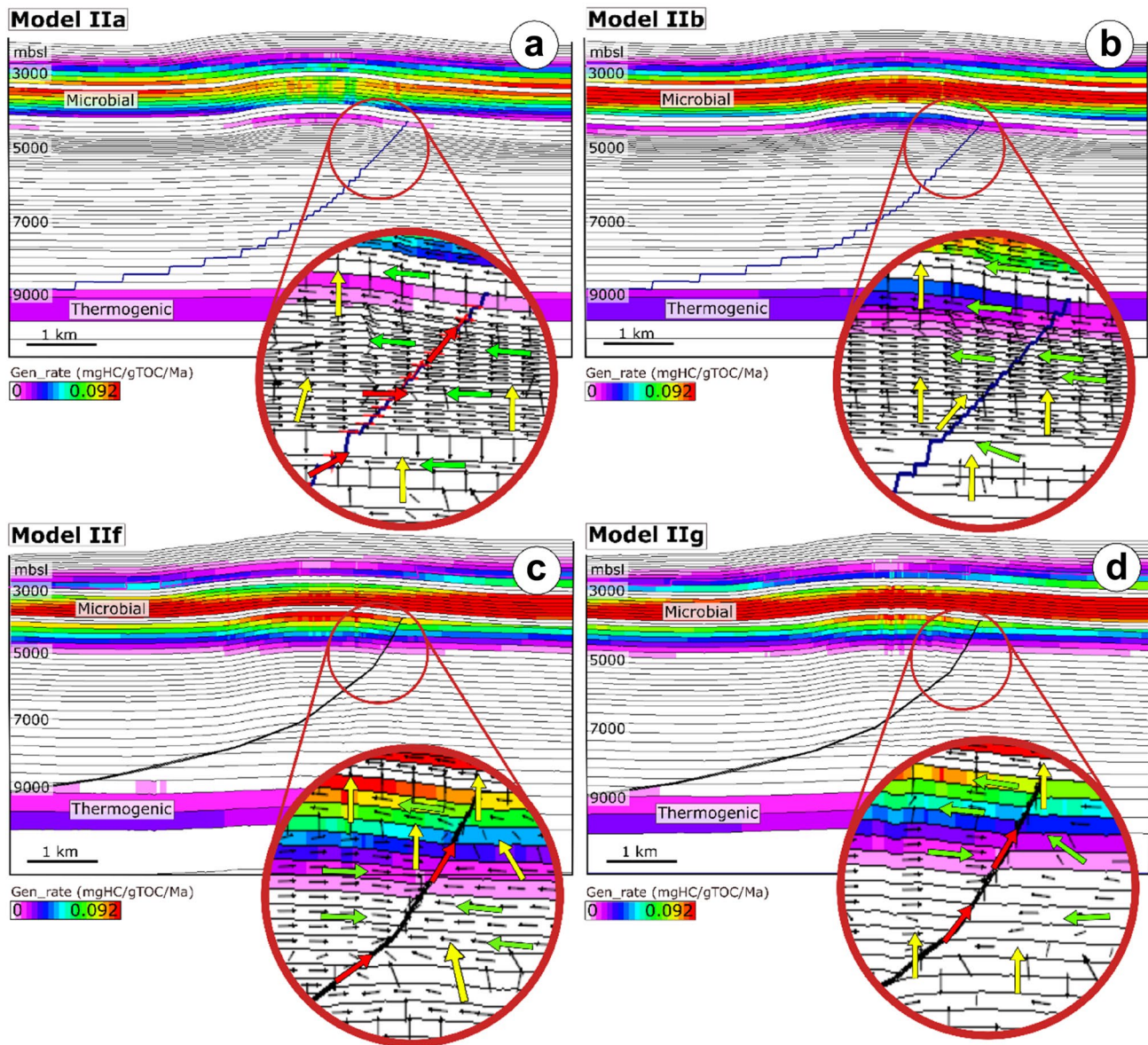


**Fig. 9** Model II: Generation rate of microbial and thermogenic methane per total organic carbon (TOC) mass (Gen\_rate). The generation rate of methane is measured as mass in milligrams (mg) per total mass of organic carbon (gTOC) per million years (Ma). Enlarged sections show overlaid fluid flow vectors, green arrows = along strata

flow, red = fault flow, yellow = vertical flow. **a** Model IIa: Fault open to flow; **b** Model IIb: fault closed to fluid flow; **c** Model IIc: 3-layer fault with open core and closed damage zone; **d** Model IIg: 3-layer fault with closed core and open damage zone

more complex deformation and smaller anticlinal structures, as seen in Model I. This is consistent with Crutchley et al. (2019), who observed that the more pronounced the anticlinal ridges are, the greater the influence of other factors such as ridge erosion, forearc sub-basin formation and gas recycling at the BGHS.

Where fault zones facilitate upward vertical flow, either along the fault core or the associated damage zone, they create a bypass mechanism between layered strata, thereby permitting fluids to migrate between permeable layers that

might otherwise have been separated by impermeable layers. However, as stated earlier, where the fault core is impermeable, faults may also act as a baffle to horizontal fluid migration and cause a shift in areas of upward fluid flow and hydrate formation. This restricts flow and compartmentalises hydrate formation to one side of the fault, while potentially still facilitating vertical flux through the damage zone. The accretionary ridge complexes of the Hikurangi Margin are highly spatially variable, both laterally and vertically, and as such, the permeability of fault

zones is likely to vary substantially across short distances. The physical properties of fault zones may also change with time due to repeated phases of tectonic activity and diagenetic processes. As such, it is challenging to separate the two factors of faulting and folding as they are inherently connected and highly heterogeneous. The results we presented here allow us to start disentangling these factors.

## Conclusions

The models we presented demonstrate the importance of conceptual models of fluid flow through faults in the framework of gas hydrate formation. To our knowledge, these conceptual models have not previously been investigated in a quantitative manner. Thrust faults along the Hikurangi Margin play a substantial role in facilitating fluid flow from depth. Fluid flow associated with fault zones may impact fault mechanics, with fluid migration being one of the factors exerting a primary control on the generation of seismicity, low frequency earthquakes and slow slip events (Saffer and Tobin 2011; Saffer and Wallace 2015). As such, these models may help improve our understanding of much larger scale processes of fault mechanics, in addition to the more localised processes of hydrate formation and gas seepage. The key results of our study can be summarised as follows:

- Within the scope of the modelled scenarios, faults are required to act as flow pathways for fluids to reproduce the distribution of hydrate as observed in the seismic data. Where faults are closed to fluid flow, or removed from the model entirely, the amount of hydrate produced is reduced.
- Faults that are open to flow increase the saturation of hydrate around the tips of faults, particularly where faults terminate near the BGHS.
- Conversely, faults closed to flow result in flow compartmentalisation, which influences the distribution of hydrate.
- Within the geological context of our models, faults are required for channelling flow to shallower parts of the GHSZ to form shallow hydrate deposits.
- The proximity of the fault termination in the sub-seafloor (i.e., the depth of a termination beneath the BGHS) is a key controlling factor for hydrate saturation. Faults that terminate relatively deep beneath the BGHS will have little to no effect on hydrate saturation.

**Acknowledgements** This research is funded by New Zealand's Ministry for Business, Innovation and Employment, contract C05X1708. Seismic data are available at <https://data.nzpam.govt.nz>. We acknowledge the use of GLOBE Claritas® software and support from the

Claritas team. We are grateful to Schlumberger for providing access to PetroMod™ basin modelling software. We would like to thank the editor, Dr. Wu-Cheng Chi, and two anonymous reviewers for providing constructive feedback that greatly benefited the clarity of this manuscript.

## References

- Bailleul J, Chanier F, Ferrière J et al (2013) Neogene evolution of lower trench-slope basins and wedge development in the central Hikurangi subduction margin, New Zealand. *Tectonophysics* 591:152–174. <https://doi.org/10.1016/J.TECTO.2013.01.003>
- Balaman SY (2019) Decision-making for biomass-based production chains. Elsevier, Amsterdam
- Barnes PM, Lamarche G, Bialas J et al (2010) Tectonic and geological framework for gas hydrates and cold seeps on the Hikurangi subduction margin, New Zealand. *Mar Geol* 272:26–48. <https://doi.org/10.1016/J.MARGE.2009.03.012>
- Biros D, Cuevas R, Moehl B (1995) Well completion report, Titihaeo-1, PPL38318: PR2081. Wellington, New Zealand
- Bland KJ, Uruski CI, Isaac MJ (2015) Pegasus Basin, eastern New Zealand: a stratigraphic record of subsidence and subduction, ancient and modern. *New Zeal J Geol Geophys* 58:319–343. <https://doi.org/10.1080/00288306.2015.1076862>
- Boswell R, Collett TS, Frye M et al (2012) Subsurface gas hydrates in the northern Gulf of Mexico. *Mar Pet Geol* 34:4–30. <https://doi.org/10.1016/j.marpetgeo.2011.10.003>
- CGG Services Ltd. (2014) PEP 54858 and PEP 54861 PEG09 PSTM reprocessing report 2014. Wellington, New Zealand
- Chatterjee S, Bhatnagar G, Dugan B et al (2014) The impact of lithologic heterogeneity and focused fluid flow upon gas hydrate distribution in marine sediments. *J Geophys Res Solid Earth* 119:6705–6732. <https://doi.org/10.1002/2014JB011236>
- Childs C, Manzocchi T, Walsh JJ et al (2009) A geometric model of fault zone and fault rock thickness variations. *J Struct Geol* 31:117–127. <https://doi.org/10.1016/j.jsg.2008.08.009>
- Choi J-H, Edwards P, Kyoungtae K et al (2016) Definition and classification of fault damage zones: a review and a new methodological approach. *Earth Sci Rev* 152:70–87. <https://doi.org/10.1016/J.EARSCIREV.2015.11.006>
- Clennell MB, Hovland M, Booth JS et al (1999) Formation of natural gas hydrates in marine sediments: 1. Conceptual model of gas hydrate growth conditioned by host sediment properties. *J Geophys Res* 104:22985. <https://doi.org/10.1029/1999jb900175>
- Cook AE, Malinverno A (2013) Short migration of methane into a gas hydrate-bearing sand layer at Walker Ridge, Gulf of Mexico. *Geochem Geophys Geosyst* 14:283–291. <https://doi.org/10.1002/ggge.20040>
- Crutchley GJ, Pecher IA, Gorman AR et al (2010) Seismic imaging of gas conduits beneath seafloor seep sites in a shallow marine gas hydrate province, Hikurangi Margin, New Zealand. *Mar Geol* 272:114–126. <https://doi.org/10.1016/j.margo.2009.03.007>
- Crutchley GJ, Fraser DRA, Pecher IA et al (2015) Gas migration into gas hydrate-bearing sediments on the southern Hikurangi margin of New Zealand. *J Geophys Res Solid Earth* 120:725–743. <https://doi.org/10.1002/2014JB011503>
- Crutchley GJ, Kroeger KF, Pecher IA et al (2017) Gas Hydrate Formation Amid Submarine Canyon Incision: Investigations From New Zealand's Hikurangi Subduction Margin. *Geochem Geophys Geosys*. <https://doi.org/10.1002/2017GC007021>
- Crutchley GJ, Kroeger KF, Pecher IA, Gorman AR (2019) How tectonic folding influences gas hydrate formation: New Zealand's



- Hikurangi subduction margin. *Geology* 47:39–42. <https://doi.org/10.1130/G45151.1>
- Duan Z, Mao S (2006) A thermodynamic model for calculating methane solubility, density and gas phase composition of methane-bearing aqueous fluids from 273 to 523 K and from 1 to 2000 bar. *Geochim Cosmochim Acta* 70:3369–3386. <https://doi.org/10.1016/J.GCA.2006.03.018>
- Field BD, Uruski CI, Beu AG et al (1997) Cretaceous-Cenozoic geology and petroleum systems of the East Coast region, New Zealand. Institute of Geological & Nuclear Sciences monograph 19 2 v. Lower Hutt, New Zealand
- Fujii T, Tin Aung T, Wada N et al (2016) Modeling gas hydrate petroleum systems of the Pleistocene turbiditic sedimentary sequences of the Daini- Atsumi area, eastern Nankai Trough, Japan. *Interpretation* 4:SA95–SA111. <https://doi.org/10.1190/INT-2015-0022.1>
- Fisher QJ, Harris SD, McAllister E et al (2001) Hydrocarbon flow across faults by capillary leakage revisited. *Mar Pet Geol* 18:251–257. [https://doi.org/10.1016/S0264-8172\(00\)00064-7](https://doi.org/10.1016/S0264-8172(00)00064-7)
- Fisher QJ, Haneef J, Grattoni CA et al (2018) Permeability of fault rocks in siliciclastic reservoirs: recent advances. *Mar Pet Geol* 91:29–42. <https://doi.org/10.1016/j.marpetgeo.2017.12.019>
- Flemings PB, Liu X, Winters GJ (2003) Critical pressure and multiphase flow in Blake Ridge gas hydrates. *Geology* 31:1057–1060
- Fugro Marine Geoservices (2015) PEP57083, PEP57085, PEP57087 integrated final report: geophysical, geochemical and heat flow survey, 2015. Wellington, New Zealand
- Fugro Seismic Imaging Pty Ltd. (2005) Bruin 2D seismic survey. East Coast Basin. Petroleum report-3414. Wellington, New Zealand
- EPI Group (2014) APB-13-2D Pegasus Basin 2D quality assurance report PEP 54861 marine 2D seismic survey PEP 54861. Wellington, New Zealand
- Hantschel T, Kauerauf AI (2009) Fundamentals of basin and petroleum systems modeling. Springer, Berlin
- Henry SA, Ellis S, Uruski CI (2003) Conductive heat flow variations from bottom-simulating reflectors on the Hikurangi margin, New Zealand. *Geophys Res Lett* 30:1065. <https://doi.org/10.1029/2002GL015772>
- Hillman JIT, Cook AE, Daigle H et al (2017) Gas hydrate reservoirs and gas migration mechanisms in the Terrebonne Basin, Gulf of Mexico. *Mar Pet Geol*. <https://doi.org/10.1016/j.marpetgeo.2017.07.029>
- Holbrook WS, Hoskins H, Wood WT et al (1996) Methane hydrate and free gas on the Blake ridge from vertical seismic profiling. *Science*. <https://doi.org/10.1126/science.273.5283.1840>
- Hornbach MJ, Saffer DM, Steven Holbrook W (2004) Critically pressured free-gas reservoirs below gas-hydrate provinces. *Nature* 427:142–144. <https://doi.org/10.1038/nature02172>
- Johnson HP, Miller UK, Salmi MS, Solomon EA (2015) Analysis of bubble plume distributions to evaluate methane hydrate decomposition on the continental slope. *Geochem Geophys Geosyst* 16:3825–3839. <https://doi.org/10.1002/2015GC005955>
- Jørgensen SE, Fath BD (2011) Concepts of modelling. In: *Developments in environmental modelling*. Elsevier, Amsterdam, pp 19–93
- Kroeger KF, Plaza-Faverola A, Barnes PM, Pecher IA (2015) Thermal evolution of the New Zealand Hikurangi subduction margin: Impact on natural gas generation and methane hydrate formation—a model study. *Mar Pet Geol* 63:97–114. <https://doi.org/10.1016/j.marpetgeo.2015.01.020>
- Kroeger KF, Crutchley GJ, Kellett R, Barnes PM (2019) A 3D model of gas generation, migration and gas hydrate formation at a young convergent margin (Hikurangi Margin, New Zealand). *Geochem Geophys Geosyst*. <https://doi.org/10.1029/2019gc008275>
- Lewis KB, Pettinga JR (1993) The emerging imbricate frontal wedge of the Hikurangi Margin. In: Ballance PF (ed) *Sedimentary basins of the world, vol 2*. Elsevier, Amsterdam, pp 225–250
- Li Y, Hou G, Hari KR et al (2018) The model of fracture development in the faulted folds: the role of folding and faulting. *Mar Pet Geol* 89:243–251. <https://doi.org/10.1016/j.marpetgeo.2017.05.025>
- Liu X, Flemings PB (2006) Passing gas through the hydrate stability zone at southern Hydrate Ridge, offshore Oregon. *Earth Planet Sci Lett* 241:211–226. <https://doi.org/10.1029/2005JB004227>
- Liu X, Flemings PB (2007) Dynamic multiphase flow model of hydrate formation in marine sediments. *J Geophys Res* 112:B03101. <https://doi.org/10.1029/2005JB004227>
- Macelloni L, Lutken CB, Garg S et al (2015) Heat-flow regimes and the hydrate stability zone of a transient, thermogenic, fault-controlled hydrate system (Woolsey Mound northern Gulf of Mexico). *Mar Pet Geol* 59:491–504. <https://doi.org/10.1016/j.marpetgeo.2014.09.010>
- Malinverno A, Goldberg DS (2015) Testing short-range migration of microbial methane as a hydrate formation mechanism: results from Andaman Sea and Kumano Basin drill sites and global implications. *Earth Planet Sci Lett* 422:105–114. <https://doi.org/10.1016/j.epsl.2015.04.019>
- Manzocchi T, Heath AE, Palanathakumar B et al (2008) Faults in conventional flow simulation models: a consideration of representational assumptions and geological uncertainties. *Pet Geosci* 14:91–110. <https://doi.org/10.1144/1354-079306-775>
- Manzocchi T, Childs C, Walsh JJ (2011) Faults and fault properties in hydrocarbon flow models. In: *Frontiers in geofluids*. Wiley/Blackwell, Oxford (10.1111), pp 94–113
- McArthur AD, Claussmann B, Bailleul J et al (2019) Variation in syn-subduction sedimentation patterns from inner to outer portions of deep-water fold and thrust belts: examples from the Hikurangi subduction margin of New Zealand. *Geol Soc Lond*. <https://doi.org/10.1144/sp490-2018-95>
- McKeown MC (2018) Understanding the physical sedimentology of the modern Madden Canyon distributary system. University of Auckland, Auckland
- Mitchell TM, Faulkner DR (2009) The nature and origin of off-fault damage surrounding strike-slip fault zones with a wide range of displacements: a field study from the Atacama fault system, northern Chile. *J Struct Geol* 31:802–816. <https://doi.org/10.1016/j.jsg.2009.05.002>
- Mitchell J, Mackay K, Neil HL et al (2012) Undersea New Zealand, 1:50,000,000. NIWA Chart, Miscellaneous Series No. 92
- Morley CK, King R, Hillis R et al (2011) Deepwater fold and thrust belt classification, tectonics, structure and hydrocarbon prospectivity: a review. *Earth Sci Rev* 104:41–91. <https://doi.org/10.1016/J.EARSCIREV.2010.09.010>
- Navalpakam RS, Pecher I, Stern T (2012) Weak and segmented bottom simulating reflections on the Hikurangi Margin, New Zealand—implications for gas hydrate reservoir rocks. *J Pet Sci Eng* 88–89:29–40
- Nole M, Daigle H, Cook AE, Malinverno A (2016) Short-range, overpressure-driven methane migration in coarse-grained gas hydrate reservoirs. *Geophys Res Lett* 43:9500–9508. <https://doi.org/10.1002/2016GL070096>
- Nole M, Daigle H, Cook AE et al (2017) Linking basin-scale and pore-scale gas hydrate distribution patterns in diffusion-dominated marine hydrate systems. *Geochem Geophys Geosyst* 18:653–675. <https://doi.org/10.1002/2016GC006662>
- Paola C, Leeder M (2011) Simplicity versus complexity. *Nature* 469:38–39. <https://doi.org/10.1038/469038a>
- Patterson JW, Driesner T, Matthai S, Tomlinson R (2018) Heat and fluid transport induced by convective fluid circulation within a fracture or fault. *J Geophys Res Solid Earth* 123:2658–2673
- Peacock DCP, Dimmen V, Rotevatn A, Sanderson DJ (2017) A broader classification of damage zones. *J Struct Geol* 102:179–192. <https://doi.org/10.1016/j.jsg.2017.08.004>

- Pecher IA, Henrys SA, Ellis S et al (2005) Erosion of the seafloor at the top of the gas hydrate stability zone on the Hikurangi Margin, New Zealand. *Geophys Res Lett* 32:L24603. <https://doi.org/10.1029/2005GL024687>
- Pecher IA, Henrys SA, Wood WT et al (2010) Focussed fluid flow on the Hikurangi Margin, New Zealand—evidence from possible local upwarping of the base of gas hydrate stability. *Mar Geol* 272:99–113. <https://doi.org/10.1016/j.margeo.2009.10.006>
- Pecher IA, Barnes PM, LeVay LJ, Expedition 372 Scientists (2018) Expedition 372 preliminary report: creeping gas hydrate slides and Hikurangi LWD
- Piñero E, Hensen C, Haeckel M et al (2016) 3-D numerical modelling of methane hydrate accumulations using PetroMod. *Mar Pet Geol* 71:288–295. <https://doi.org/10.1016/j.marpetgeo.2015.12.019>
- Plaza-Faverola A, Klaeschen D, Barnes P et al (2012) Evolution of fluid expulsion and concentrated hydrate zones across the southern Hikurangi subduction margin, New Zealand: an analysis from depth migrated seismic data. *Geochem Geophys Geosyst*. <https://doi.org/10.1029/2012gc004228>
- Power ME, Dietrich WE, Sullivan KO (1998) Experimentation, observation and inference in river and watershed investigations. In: Resetarits WJ, Bernardo J (eds) *Experimental ecology: issues and perspectives*. Oxford University Press, Oxford, pp 113–132
- Saffer DM, Tobin HJ (2011) Hydrogeology and mechanics of subduction zone forearcs: fluid flow and pore pressure. *Annu Rev Earth Planet Sci* 39:157–186. <https://doi.org/10.1146/annurev-earth-040610-133408>
- Saffer DM, Wallace LM (2015) The frictional, hydrologic, metamorphic and thermal habitat of shallow slow earthquakes. *Nat Geosci* 8:594–600. <https://doi.org/10.1038/ngeo2490>
- Saffer DM, Wallace LM, Petronotis K, Expedition 375 Scientists (2018) Expedition 375 preliminary report: Hikurangi subduction margin coring and observatories
- Sloan ED, Koh CA (2008) *Clathrate hydrates of natural gases—chemical industries*. CRC Press, Boca Raton
- Taladay K, Boston B, Moore G (2017) Gas-in-place estimate for potential gas hydrate concentrated zone in the Kumano Basin, Nankai Trough Forearc, Japan. *Energies* 10:1552. <https://doi.org/10.3390/en10101552>
- Tap Oil Ltd. (2004) Tawatawa-1 well completion report: PR3067. Wellington, New Zealand
- Tishchenko P, Hensen C, Wallmann K, Wong CS (2005) Calculation of the stability and solubility of methane hydrate in seawater. *Chem Geol* 219:37–52
- Torabi A, Berg SS (2011) Scaling of fault attributes: a review. *Mar Pet Geol* 28:1444–1460. <https://doi.org/10.1016/J.MARPE.TGEO.2011.04.003>
- Townend J, Sutherland R, Toy VG et al (2017) Petrophysical, geochemical, and hydrological evidence for extensive fracture-mediated fluid and heat transport in the Alpine fault's hanging-wall damage zone. *Geochem Geophys Geosyst* 18:4709–4732. <https://doi.org/10.1002/2017GC007202>
- Ungerer P (1990) State of the art of research in kinetic modelling of oil formation and expulsion. *Org Geochem* 16:1–25. [https://doi.org/10.1016/0146-6380\(90\)90022-R](https://doi.org/10.1016/0146-6380(90)90022-R)
- Uruski CI (2010) New Zealand's deepwater frontier. *Mar Pet Geol* 27:2005–2026. <https://doi.org/10.1016/j.marpetgeo.2010.05.010>
- Walcott RI (1978) Present tectonics and Late Cenozoic evolution of New Zealand. *Geophys J Int* 52:137–164. <https://doi.org/10.1111/j.1365-246X.1978.tb04225.x>
- Wang H, Crutchley GJ, Stern T (2017) Gas hydrate formation in compressional, extensional and un-faulted structural settings—examples from New Zealand's Hikurangi margin. *Mar Pet Geol* 88:69–80. <https://doi.org/10.1016/j.marpetgeo.2017.08.001>
- Weinberger JL, Brown KM (2006) Fracture networks and hydrate distribution at Hydrate Ridge, Oregon. *Earth Planet Sci Lett* 245:123–136. <https://doi.org/10.1016/j.epsl.2006.03.012>
- Wibberley CAJ, Shimamoto T (2003) Internal structure and permeability of major strike-slip fault zones: the Median Tectonic Line in Mie Prefecture, Southwest Japan. *J Struct Geol* 25:59–78
- Yielding G, Freeman B, Needham DT et al (1997) Quantitative fault seal prediction. *Am Assoc Pet Geol Bull* 81:897–917. <https://doi.org/10.1306/522B498D-1727-11D7-8645000102C1865D>
- You K, Kneafsey TJ, Flemings PB et al (2015) Salinity-buffered methane hydrate formation and dissociation in gas-rich systems. *J Geophys Res Solid Earth* 120:643–661. <https://doi.org/10.1002/2014JB011190>
- You K, Flemings PB (2018) Methane hydrate formation in thick sandstones by free gas flow. *J Geophys Res Solid Earth* 123:4582–4600. <https://doi.org/10.1029/2018JB015683>

**Publisher's Note** Springer Nature remains neutral with regard to jurisdictional claims in published maps and institutional affiliations.